Technical Article

Automated Pleural Line Detection Based on Radon Transform Using Ultrasound

Ultrasonic Imaging
2021, Vol. 43(1) 19–28

DOI: 10.1177/0161734620976408
journals.sagepub.com/home/uix
SAGE

Jiangang Chen[1*], Jiawei Li[2,3*], Chao He[4*], Wenfang Li[4], and Qingli Li[1]

Abstract

It is of vital importance to identify the pleural line when performing lung ultrasound, as the pleural line not only indicates the interface between the chest wall and lung, but offers additional diagnostic information. In the current clinical practice, the pleural line is visually detected and evaluated by clinicians, which requires experiences and skills with challenges for the novice. In this study, we developed a computer-aided technique for automated pleural line detection using ultrasound. The method first utilized the Radon transform to detect line objects in the ultrasound images. The relation of the body mass index and chest wall thickness was then applied to estimate the range of the pleural thickness, based on which the pleural line was detected together with the consideration of the ultrasonic properties of the pleural line. The proposed method was validated by testing 83 ultrasound data sets collected from 21 pneumothorax patients. The pleural lines were successfully identified in 76 data sets by the automated method (successful detection rate 91.6%). In those successful cases, the depths of the pleural lines measured by the automated method agreed with those manually measured as confirmed with the Bland-Altman test. The measurement errors were below 5% in terms of the pleural line depth. As a conclusion, the proposed method could detect the pleural line in an automated manner in the defined data set. In addition, the method may potentially act as an alternative to visual inspection after further tests on more diverse data sets are performed in future studies.

Keywords

lung, ultrasound, pleural line identification, image processing, automated measurement

Introduction

The pleura is the lining of the lung and often appears as a bright line in ultrasound scans. As a key anatomical landmark, the pleural line plays an important role in lung ultrasound. It not only indicates the interface between the chest wall and lung anatomically, but associates with many lung pathologies, for example, pleura thickening and pleural effusion.[1-3] The detection of the pleural line is the starting point for evaluating several ultrasonic features of the lung,[1,3-6] including (i) lung sliding that appears at the pleurae as part of pneumothorax examinations[7]; (ii) B line that starts from the pleural line for evaluating the pulmonary edema and fibrosis[8-10]; and lung pulse that is associated with the heart activity at the pleural line.[11] Pleural line is also the basis for the diagnosis of pleural diseases and guiding the interventional therapy, such as ultrasound-guided needle biopsy (UGNB).[2,3,12]

Currently, the detection and evaluation of the pleural line are conventionally through visual ultrasonography which, however, has some limitations. Firstly, the pleural line is easily mistaken for the interface of the chest muscle and fat layer on the ultrasound images. Secondly, the pleural line may show irregular shapes under pathologies, making its evaluation time-consuming and experience-dependent.[1] Thirdly, the quantitative assessment of the pleurae is difficult, for example, measuring the pleurae thickness, especially when the pleurae is unclear at pathological status.[1,7] A method for

[1]Shanghai Key Laboratory of Multidimensional Information Processing, East China Normal University, Shanghai, China
[2]Department of Medical Ultrasound, Fudan University Shanghai Cancer Center, Shanghai, China
[3]Department of Oncology, Shanghai Medical College, Fudan University, Shanghai, China
[4]Department of Emergency and Critical Care, Changzheng Hospital, Naval Medical University, Shanghai, China

*Jiangang Chen, Jiawei Li, and Chao He equally contributed to the work.

Corresponding Authors:
Qingli Li, Shanghai Key Laboratory of Multidimensional Information Processing, East China Normal University, #500 Dongchuan Rd., Shanghai 200241, China.
Email: qlli@cs.ecnu.edu.cn

Wenfang Li, Department of Emergency and Critical Care, Changzheng Hospital, Naval Medical University, #415 Fengyang Rd., Shanghai 200003, China.
Email: chzhedlwf@163.com

Table 1. Patent Information.

P	1	2	3	4	5	6	7	8	9	10	11	12	13	14	15	16	17	18	19	20	21
A	38	27	45	49	26	60	29	55	49	32	33	47	33	36	39	28	56	38	43	44	29
S	M	F	F	M	M	F	M	M	F	M	M	M	F	F	M	F	M	F	M	F	F
H	1.65	1.74	1.60	1.72	1.63	1.59	1.76	1.68	1.69	1.78	1.64	1.73	1.61	1.72	1.80	1.56	1.75	1.62	1.68	1.58	1.59
W	52.0	70.0	55.4	67.7	54.8	53.3	77.8	83.9	64.3	84.3	64.9	74.6	67.7	81.7	91.7	90.1	94.0	91.4	91.7	68.1	82.9
B	19.1	23.1	21.6	22.9	20.6	21.1	25.1	29.7	22.5	26.6	24.1	24.9	26.1	27.6	28.3	37.0	30.7	34.8	32.5	27.3	32.8
C	15.6	19.2	18.3	20.3	14.5	17.3	24.3	30.5	16.3	22.2	19.8	22.8	21.0	25.4	26.0	33.4	31.5	35.7	28.2	27.3	34.6

Note. P = patient; A = age; S = sex; H = height (m); W = weight (kg); B = body mass index; C = chest wall thickness (mm).

automated pleural line detection could not only make the detection of the pleural line objective but also realize quantitative assessment of the pleurae. In addition, the automated detection of the pleural line may contribute to the diagnosis of some pleural diseases, including pleural inflammation,[13] pleural fibrosis,[14] and pleural thickening,[15] as well as some guidance procedure, like UGNB.[12]

On the other hand, ultrasound automation has recently drawn great attention in virtue of the operator-dependent nature of ultrasound. Many smart algorithms have been developed for automated ultrasound measurement for different parameters, for example, blood vessel diameter and wall thickness.[8,16-23] Biswas et al.[17] applied deep learning for automated lumen characterization of carotid artery using ultrasound. Our previous work focused on developing smart algorithms for automated inferior vena cava identifications[22] and measurements.[21] In the field of lung ultrasound, endeavors were focused on the detection of different lung ultrasound artifacts, for example, B-lines and pleural lines. Brusasco et al.[8] and Moshavegh et al.[24] attempted to provide quantitative measure for the number of B-lines present in lung ultrasound images. Moshavegh et al.[25] attempted to delineate the pleural line based on the confidence map estimation in which the random walks framework considering ultrasound specific constraints was adopted. Anantrasirichai et al.[26] applied the Radon and Hough transforms to identify line objects in an ultrasound image, and then differentiate the pleural line, B-line, A-line, and Z-line with several constraints that were artificially determined in part.

Toward automated pleural line detection with least human decision, in this study, we proposed a method for automated pleural line detection based on the Radon transform, taking advantages of the anatomical and ultrasonic properties of the pleural line. As an innovation, the relation of the body mass index (BMI) and chest wall thickness (CWT) was considered as the input for the proposed algorithm for accurate pleural line detection.

Materials and Methods

Subjects

Twenty-one pneumothorax patients with moderate injuries (the air pocket occupied part of the left or right lung as CT confirmed) were enrolled in the study with the height and weight recorded, as listed in Table 1. An ultrasound machine CX50 (Philips Healthcare, Bothell, US) equipped with a linear probe (L12-3, central frequency 7.5 MHz) working under the penetration mode were used for data collection at a frame rate of 25 frame per second. Note that in the penetration mode the transmit frequency of the probe is close to the lower edge of the frequency range to enhance the penetration of the ultrasound waves. The patients were asked to sit or stand during the data collection. Two clinicians with more than 6 years' experience in ultrasound conducted the study, with one (Clinician A) performed the ultrasound scan and the other (Clinician B) interpreted the collected data. Ultrasound cine loops with a duration of 4 seconds were collected in transverse scans in the anterior upper and lower chest areas of both sides of each patient following the BLUE Protocol.[2,27] Data collections were repeated three times at each area, resulting in 83 datasets (249 ultrasound cine loops) in terms of the measurement site with one excluded due to the poor image quality. Note that the image data collected from a patient included at least one for pneumothorax which was confirmed by Clinician A. The collected data thus included at least two important types of lung conditions, that is, lung sliding (normal) and no lung sliding (pneumothorax).[28] All the ultrasound images were collected with the requirement that the pleural line should be under good visualization and occupy more than 2/3 of the width of the screen. The data sets were stored in the format of dynamic digital imaging and communications in medicine. A group of 16 consecutive ultrasound frames (denoted as *Group-16*) was randomly selected from each cine loop for the following manual and automated measurements. The study was approved by the ethics committee of East China Normal University, Shanghai, China. All patients provided written informed consents.

Manual Pleural Line Detection

The pleural line in each cine loop was randomly and blindly detected on the first frame of *Group-16* by Clinician B. As an example, Figure 1(a) representatively shows an ultrasound image with the pleural line displayed (indicated by an arrow in the figure). The depth of the detected pleural line was

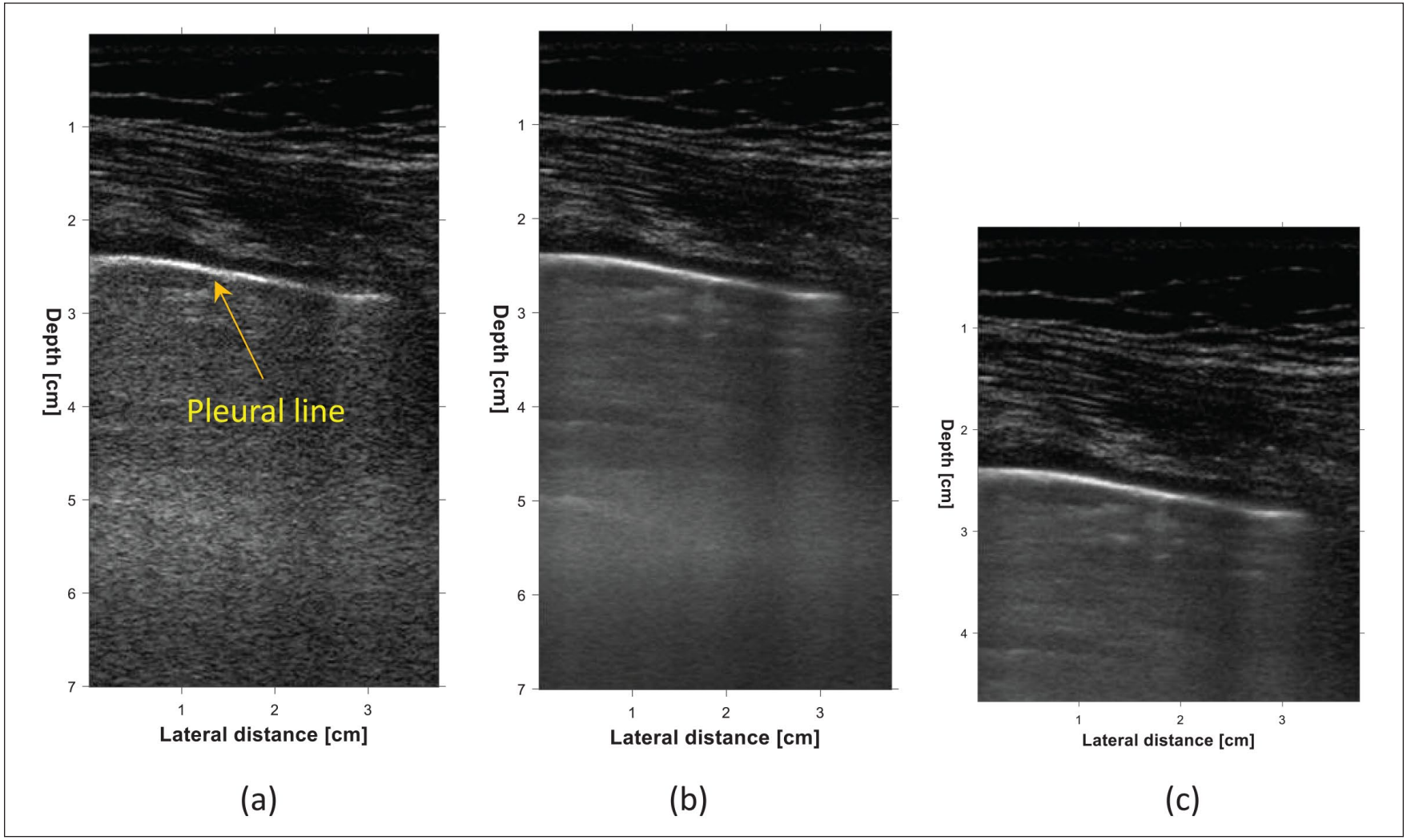

Figure 1. The ultrasound images showing the pleural line. (a) A single frame. (b) An averaged image. (c) The image of reduced size.

manually measured along the middle line of the image width. The measured depths in each data set (containing three cine loops) were averaged as the depth of the corresponding measured site, and subsequently compared with those measured used the automated method.

Automated Pleural Line Detection

In the automated approach, each *Group-16* was averaged to create an averaged 2D ultrasound image (Figure 1(b)). This operation could avoid the case that the pleural line is unclear or missing in some frames of the group, and make the image more smooth that facilitated the following image processing. Then the Radon transform was applied to detect the line objects on the ultrasound image as the candidates of the pleural line.

Radon transform. The Radon transform is widely applied to detect lines, circles, or ellipses in kinds of images.[29,30] In automated analysis of digital images, edge detectors can be used as a pre-processing step to obtain points or pixels that belong to the desired curves. However, there may be missing points or pixels on the desired curve, and spatial deviations between the ideal line/circle/ellipse and the noisy edge points. The purpose of the Radon transform is to perform grouping of the extracted edge features to an appropriate set of lines, circles, or ellipses.[31]

The Radon transform is an integral transform. It performs a line integrate to a function $f(x,y)$ which is defined on a two-dimensional plane along any line on a plane. It is equivalent to do CT scans. As a basic application, the Radon transform is used to reconstruct $f(x,y)$ before projection based on the transmitted light intensity of CT.

Consider $f(x,y)$ have compact support in R^2, the Radon transform is defined as

$$R(s,a)=\iint_{R^2} f(x,y)\delta(x\cos\alpha+y\sin\alpha-s)dxdy \qquad (1)$$

where R is the Radon transform operator, s is the distance of a line to the origin, α is the angle of the line referring to the direction of x^+.

Procedure of automated algorithm. The Radon-transform-based method was developed for automated pleural line detection using Matlab (The MathWorks, Natick, MA, USA). The method comprises the following steps:

1. Removing one third of Figure 1(b) vertically from the lower end of the image, as shown in Figure 1(c). Note that the removal of part of the image that is not likely to contain the pleural line would reduce the computation load, which may make the algorithm eligible for mobile ultrasound that has limited computing resources.

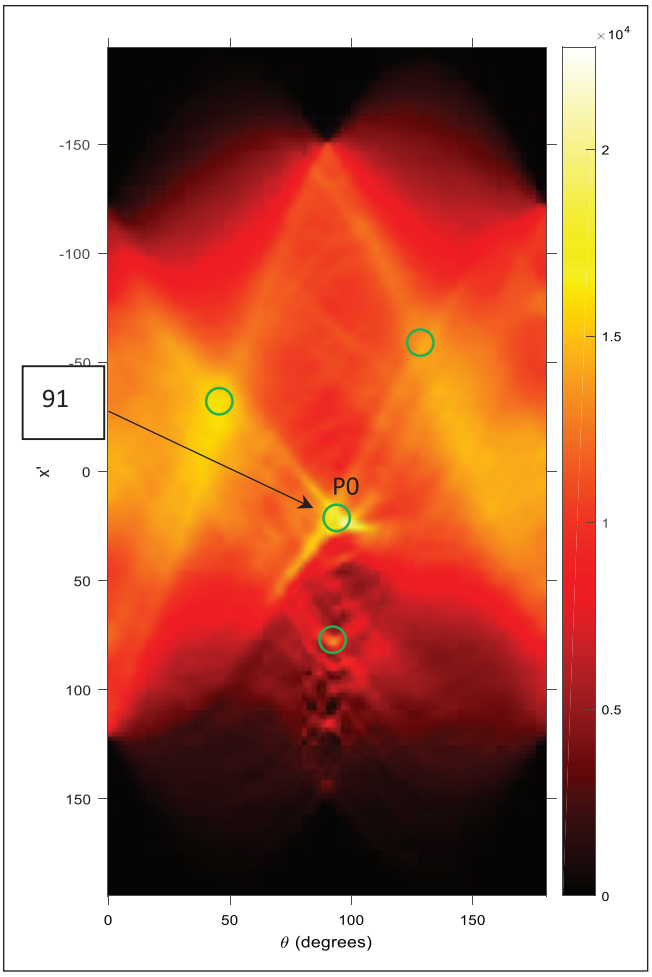

Figure 2. The intensity image of Radon transform of Figure 1.

2. Applying the Radon transform to Figure 1(c) to obtain an intensity image (Figure 2). The peaks in the figure (indicated as green circle) corresponded to line objects in Figure 1(c) which served as candidates of the pleural line. Note that the x coordinate of a peak in the figure indicated the angle of the corresponding line in Figure 1(c) according to the direction of x^+. While the y coordinate of a peak indicated the intercept of the corresponding line in Figure 1(c) with the coordinate origin being the center of the figure. Thus, the depth of a line in Figure 1(c) can be derived with the x and y coordinates of its corresponding peak in Figure 2.
3. With the above information, the peak corresponding to the pleural line was picked up from all the candidates by considering the following pre-knowledge:
   (a) The pleural line was most continuous across the screen among other candidates. As a result, the gray value of the peak corresponding to the pleural line is normally high, ranking top positions among all the peaks;

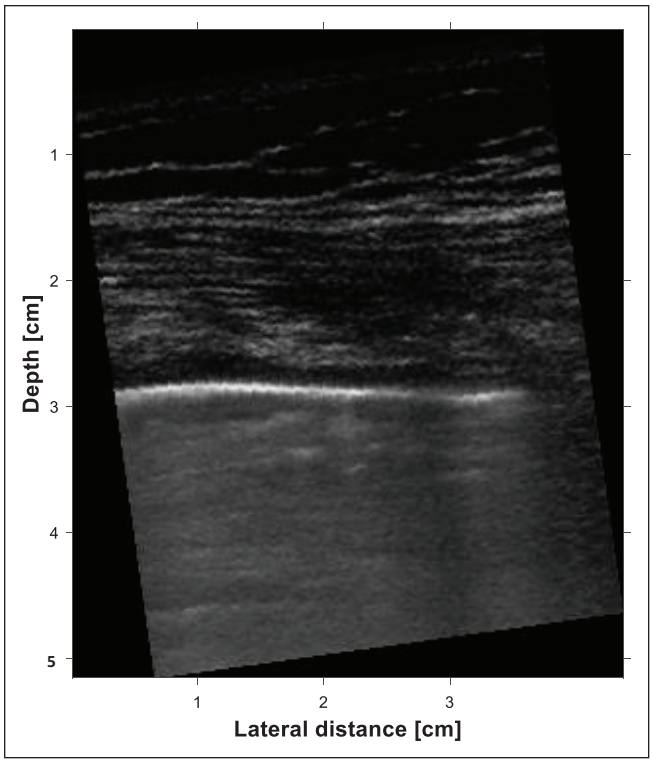

Figure 3. The rotated image of Figure 2 with the pleural line horizontally placed.

(b) The depth of the pleural line is equal to the CWT.[3] A personalized CWT could be estimated via a linear relationship of the BMI (defined as $\frac{W}{H^2}$, where W and H is weight [in kilograms] and height [in meters], respectively), and CWT (details please refer to Graphs 1 and 2 in (3)). With the range of the possible depths of the pleurae, the searching range of the pleural line could be much shrunk, facilitating the localization of the pleural line.

With the above process, the peak for the pleural line was picked up and indicated as P_0 in Figure 2. The angle of the pleural line is $\theta = 91°$ in the case as displayed in Figure 2.

4. Applying the rotation algorithm in Matlab (i.e., "imrotate[F, θ_{rotation}]," where F represents the image data to process, $\theta_{\text{rotation}} = 90 - \theta$) to Figure 1(c). A new rotated image was obtained and shown in Figure 3 in which the pleural line is horizontally placed.
5. Summing the pixel's gray values of Figure 3 along the transverse direction to obtain a lateral intensity projection curve (denoted as LIPC-1, blue line in Figure 4). For the sake of comparison, the lateral intensity project curve of Figure 1(c) is also plotted in Figure 4 (denoted as LIPC-2, red dash line in Figure 4). The peak of the projection curve corresponding to the pleural line could be located automatically with the positional information of P0 in Figure 2. In this case, the max peak of either LIPC-1 or LIPC-2 corresponded to the extracted pleural line. In addition, the peak for the pleural line in LIPC-1 is much higher than that in LIPC-2, indicating that the rotation method could highlight the position of the pleural line.
6. Extracting two troughs beside the peak for the pleural line in LIPC1 as indicated by two dash lines in Figure 4. The range between the two troughs (i.e., [2.72, 3.07]) is the lateral projection range of the pleural line. Thus, the pleural line could be automatically extracted by locating the pixel of maximum gray value within the corresponding range in Figure 3. Figure 5 shows the detection result with the pleural line highlighted by a red line.
7. Rotating Figure 3 to the original angle together with the identified pleural line, as shown in Figure 6. The depth of the pleural line was automatically measured in the middle of the image width, which is in line with the manual measurement.

The steps of the above procedure were performed automatically in the study. The proposed method for pleural line detection could be considered as fully automated. The measured depths of the pleural lines in each data set using the automated approach were averaged and compared with those manually measured.

Statistics. The repeatability of three manual and automatic measurements at the same measurement site was tested using intra-class correlation coefficient (ICC) with its 95% confidence interval (CI) calculated with SPSS 22.0 for Windows system (SPSS Inc., Chicago, IL, USA). Considering the repeated measurement, the two-way mixed effect model with the consistency option ICC (3, k) was utilized.[28] Bland-Altman analysis was used to plot the difference of manual and automatic measurements against their mean values to investigate the agreement between the manual and automatic measurements for pleural lines. The mean difference between the manual and automatic measurements ($\bar{d}$), the standard deviation of $\bar{d}$ ($SD_{\bar{d}}$), the standard error of $\bar{d}$ ($SE_{\bar{d}}$), the 95%CI of $\bar{d}$, the coefficient of repeatability (CR), and the 95% limits of agreement were calculated.

Results

In this study, the pleural lines were successfully identified in 76 data sets using the automated method (successful rate 91.6%). While the clinician identified pleural lines in all the data sets (successful rate 100%). Taking the average of three measurements in each data set as the depth at the

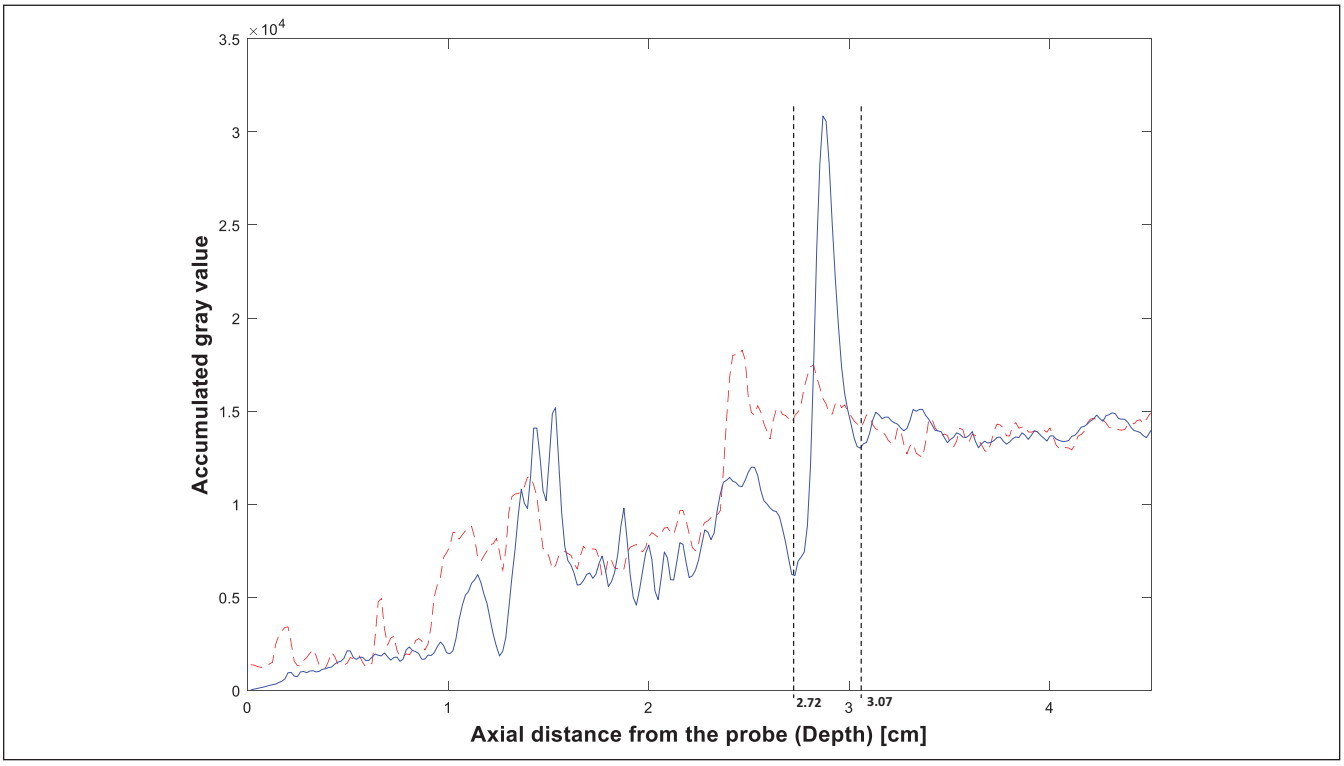

Figure 4. The lateral intensity projection curve of Figure 1 (red dash line) and Figure 3 (blue line). For interpretation of the references to colors in this figure legend, refer to the online version of this article.

measurement site, Figure 7(a) shows all the depths of the pleural lines measured using automated and manual methods. The accuracy of the automated method is shown in Figure 7(b) with the manual measurement as the gold standard. The ICC value was 0.986 (95%CI 0.979–0.991) for the three repeated measurements with the manual method and 0.998 (0.997–0.999) for the three repeated measurements with the automated method. The agreement of the automated and manual methods in measuring the depth of the pleural line was analyzed via Bland-Altman as shown in Figure 8 and Table 2. All data points were within the 95% limits of agreement. Indicated by the 95% limits of agreement, the difference between automatic and manual measurements was less than 0.92 cm. The maximum measurement error was less than 5%. Figure 9 representatively shows two images in which the proposed algorithm failed to detect the pleural lines.

Discussion

In this study, we developed a method for automated detection of the pleural line using the Radon transform. The innovation of the study included the application of a personalized constraint (i.e., the BMI-CWT relationship) together with the ultrasonic visualization of the pleura for precise detection of the pleural line. With further tests on a more diverse data set, the proposed method may potentially increase the confidence

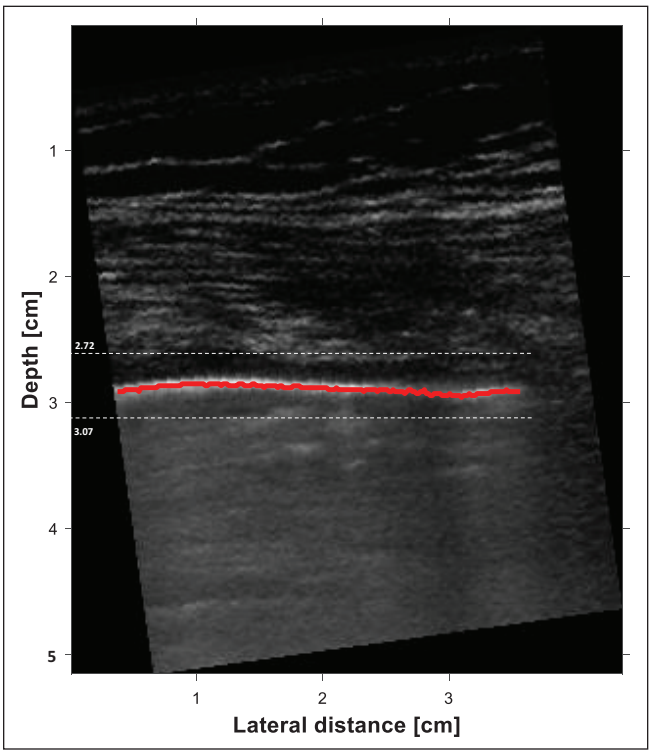

Figure 5. The rotated image with the identified pleural line highlighted by a red line (two dash lines indicate the lateral projection range of the pleural line). For interpretation of the references to colors in this figure legend, refer to the online version of this article.

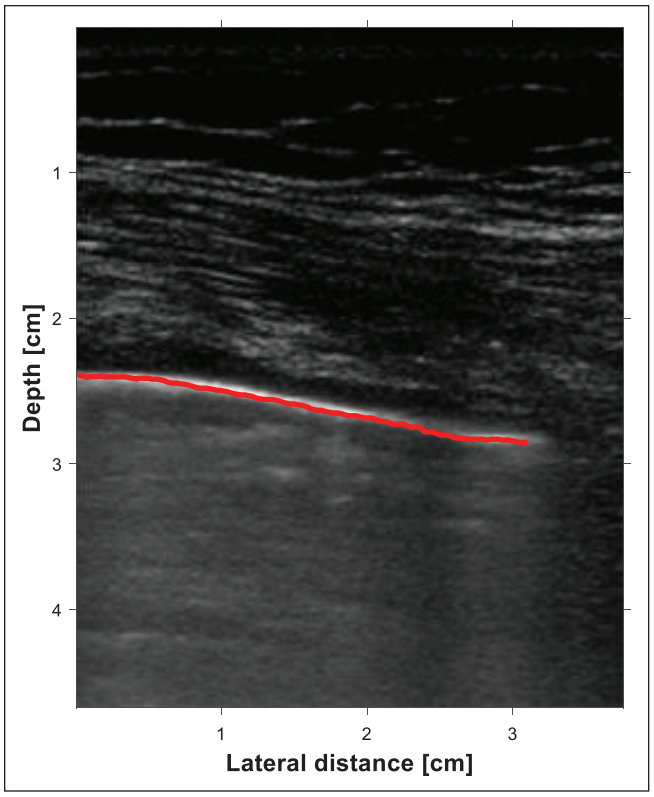

Figure 6. The original image with the pleural line identified (the pleural line is highlighted by a red line). For interpretation of the references to colors in this figure legend, refer to the online version of this article.

of inexperienced users for daily clinical practice and improve the efficiency of the clinical procedures. In addition, the automated pleural line identification is fundamental to many other smart methods that can be implemented in the area of lung ultrasound.

The method was evaluated by testing 83 data sets collected from 21 pneumothorax patients. The successful identification rate for pleural lines is 91.6% using the automatic method. This is comparable with the previous study conducted by Anantrasirichai et al.[26] in which a similar accuracy was achieved for detection of the pleural line in 100 lung ultrasound images. Furthermore, the depths of the detected pleural lines measured using the automated method were comparable with those manually measured, as shown in Figure 7(a). It could be seen that the depths of the pleural lines measured by the automated approach were close to those manually measured except for those failure cases. The measurement errors of the automated method were below 5% for the successful cases, as indicated in Figure 7(b). Automated and manual measurements also showed good agreement as analyzed by Bland-Altman shown in Figure 8. It thus validated the proposed method as a potential alternative to the manual method, although the automated method failed in detecting the pleural line in seven data sets (failure rate 8.4%).

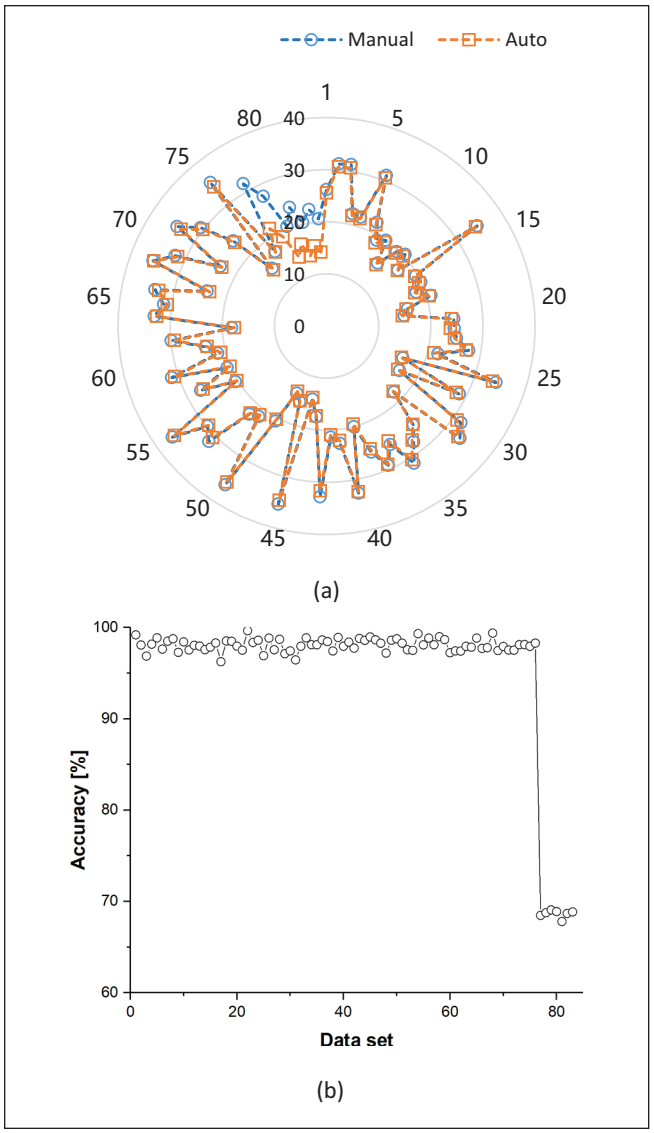

Figure 7. (a) Pleural depths measured by manual (blue circle) and automated (orange rectangle) methods. (b) accuracy of the automated method. For interpretation of the references to colors in this figure legend, refer to the online version of this article.

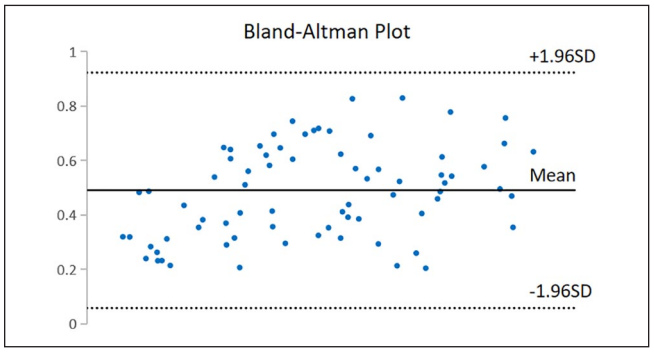

Figure 8. Bland-Altman plot of the automated approach referencing to the manual method.

Table 2. Bland-Altman Analysis for the Depth Measurement of Pleural Line in Terms of Agreement Between the Manual and Automated Methods.

	Mean	$\bar{d}$	$SD_{\bar{d}}$	$SE_{\bar{d}}$	95%CI of $\bar{d}$	*CR*	95% Limits of agreement
Manual-automated	24.72	0.49	0.22	0.03	0.44 to 0.54	2.39	0.06 to 0.92

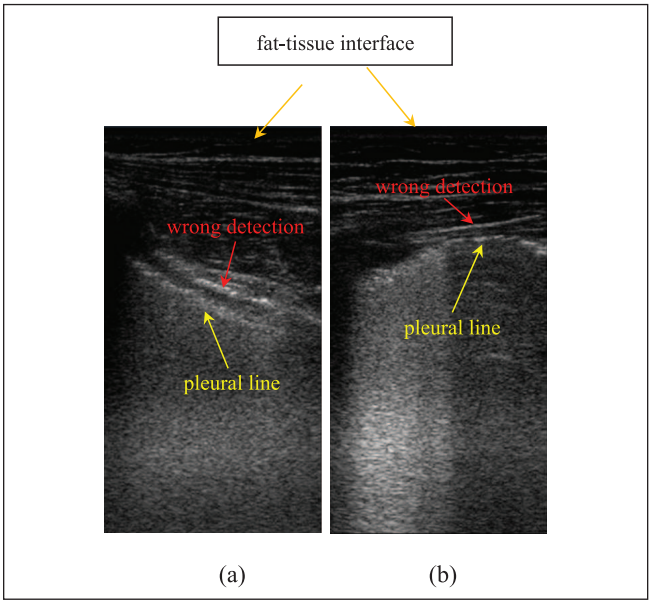

Figure 9. Failure cases in which the proposed approach failed to detect the pleural line. (a) No pleural line detected. (b) Wrong detection.

Normally the lung is identified by respiration-related movements of the visceral pleura, that is, lung sliding.[1] However, when the lung is abnormal, like the pneumothorax, the lung sliding is missing. Under such a circumstance, the identification of the lung is most dependent on the visualization. In addition, the pleural line was easily mistaken for other reflection interfaces on ultrasound images, such as the muscle fibers, fat-muscle interface, and fascia. Experiences and skills were thus required for identifying the pleura, and then the lung. In this respect, with an attempt to offer an approach for automated pleural line detection, this study could help the inexperienced clinicians to identify the pleurae and build confidence when the automated approach agreed with the visual detection.

The proposed approach for the automated detection of pleural lines may contribute to the diagnosis of some pleural diseases. For example, in pleural inflammation, the pleurae may have irregular margins in ultrasound visualization[13]; in pleural fibrosis, the pleural line may show mixed echogenic or hypoechoic appearance that did not vary in shape and location[14]; in pleural thickening, the pleural line may displayed as a belt with lower echogenicity than that in normal cases[15]; in pleural neoplasia, an appearance of round or oval-shaped, well encapsulated or demarcated mass may indicate as benign lesions, while that of thickening of the pleurae with irregular outline and a heterogeneous echo pattern may indicate as malignant lesions.[32] Thus, identification of the pleural line in an automated manner may assist in the diagnosis of those diseases. Taking the pleural thickening as an example, the distance between the two troughs as highlighted by two dash lines in Figure 4 may indicate the pleural thickness, which could be further used for the evaluation of the pleural thickening, a significant indicator for pleurisy.

In addition, the detection of pleural line may be beneficial to the procedure of UGNB. The differentiation between benign tumors and malignancies for neoplasitic pleural diseases is commonly associated with UGNB.[12] However, the tendency of the tissue lesions to dislocate under the pressure of the needle due to its elastic property increases the challenge for UGNB.[1] In this regard, automated pleural line detection may offer a real-time feedback of the position of the target, which may not only help optimize the guidance procedure and elevate the confidence of the clinicians, but increase the success rate of the biopsy. In addition, the proposed approach may provide assistant information to guide the medical robot to perform automated needle biopsy.

Moreover, the proposed method may provide fundamental technical reference for developing advanced automation techniques for pulmonary diagnosis. For example, a recent study conducted automated B-line counting[8] and lung sliding quantification.[33] The approach for automated pleural line detection may contribute to the work since the pleura is the start of the B line and where the lung sliding takes place.

In this study, the proposed automated approach failed to detect the pleural line in seven data sets. The failure cases can be divided into two categories: (1) the pleura was of lower echogenicity (Figure 9(a)), and (2) the pleural line was discontinued (Figure 9(b)), as representatively demonstrated in Figure 9. In those cases, the pleural line was mistaken for other tissues, for example, the muscle fibers. The failure cases may be attributed to inadequate scanning angles or pressures of the probe or pathologies of the pleurae, for example, pleural effusion.

The primary computation load of the proposed method is the Radon transform which could be much optimized by reducing the size of the input image. In this regard, the reduction of the size of the input image as described in Step-1 of "Procedure of Automated Algorithm" could be performed more precisely. That's to say, more portions of the original image could be removed to reduce the computing load, taking advantage of the knowledge of BMI-CWT relationship.[3] With optimization in

computation load, the proposed approach is expected to be used with mobile ultrasound instrument which has limited computing resources. On the other hand, also capable of line detection, the Hough transform is of faster processing speed than the Radon transform.[34] However, the reason why the Hough transform was not chosen for the current study relied on the considerations that (i) applying the Hough transform is not straightforward in noisy images, particularly for multiplicative speckle noise, such as the ultrasound images; (ii) the Hough transform requires the processed image to be binarized which may be not appropriate for the current study where the lung ultrasound images are of low contrast.[26]

In the study, the ultrasound machine was set as the penetration mode with the central frequency of the probe in the lower range, approximately around 3.5 MHz. Such an operation was under the consideration that the pleural line is most appeared among other structures on ultrasound images at the frequency of 3.5 MHz.[35] This contributed to the high success rate in the pleural line detection in the study. However, more lines may be displayed in higher frequency range, for example, the chest muscle fibers. In those cases, the proposed method may warrant further improvement.

There are some limitations of the study. Firstly, only the transverse scan was adopted to collect ultrasound data in the study. While in the longitudinal view, considering the rib shadows may affect the applicability of the proposed approach, improvement to the algorithm may be warranted for the accurate detection of the pleura. Secondly, the data tested in this study were collected under good control with the pleurae under good visualization and shown as micro-curved line. Thirdly, the data used for validating the presented algorithm is not general, for example, the pleural lines covered at least two third of the lateral width of the image. Such an appearance was unusual and not generally expected in general clinical scan sessions, potentially limiting the utility of the performance evaluation of the algorithm presented. Fourthly, considering the failure cases in the study, the proposed approach may be inappropriate to be used when the pleural line is unclear or discontinued, or with other artifacts that may be encountered in practice. In summary, the study is limited in its scope and general utility to the field.

In our continued future studies, the general performance of the proposed algorithm will be thoroughly analyzed based on data of larger scope toward clinical applications.

Conclusions

Detection of the pleural line is of vital importance when performing lung ultrasound. In this study, we developed an automated approach for pleural line detection using the Radon transform in pneumothorax patients. The proposed method could detect the pleural line in an automated manner in the defined data set, and potentially act as an alternative to visual inspection with further tests on more diverse data sets in future studies. We do not guarantee that the proposed method in the study is the best, but wish this work evoke efforts in the direction of ultrasound automation, in particular for the lung ultrasound.

Declaration of Conflicting Interests

The author(s) declared no potential conflicts of interest with respect to the research, authorship, and/or publication of this article.

Funding

The author(s) disclosed receipt of the following financial support for the research, authorship, and/or publication of this article: This work is supported in part by the National Natural Science Foundation of China (61975056), the Shanghai Natural Science Foundation (19ZR1416000), the Science and Technology Commission of Shanghai Municipality (20440713100, 19511120100), Key Research Fund of Logistics of PLA (Grant No. BWS14C018), and Shanghai Health and Family Planning Commission (Grant No. 2016ZB0201). The authors would like to thank the reviewers in advance for their comments and suggestions.

ORCID iD

Qingli Li https://orcid.org/0000-0001-5063-8801

References

1. Dietrich CF, Mathis G, Cui XW, Ignee A, Hocke M, Hirche TO. Ultrasound of the pleurae and lungs. Ultrasound Med Biol. 2015;41(2):351-65.
2. Gargani L, Volpicelli G. How I do it: lung ultrasound. Cardiovasc Ultrasound. 2014;12(1):25.
3. McLean AR, Richards ME, Crandall CS, Marinaro JL. Ultrasound determination of chest wall thickness: implications for needle thoracostomy. Am J Emerg Med. 2011;29(9):1173-7.
4. Manson WC, Bonz JW, Carmody K, Osborne M, Moore CL. Identification of sonographic B-lines with linear transducer predicts elevated B-type natriuretic peptide level. West J Emerg Med. 2011;12(1):102-6.
5. Copetti R, Soldati G, Copetti P. Chest sonography: a useful tool to differentiate acute cardiogenic pulmonary edema from acute respiratory distress syndrome. Cardiovasc Ultrasound. 2008;6(1):16.
6. Anderson KL, Fields JM, Panebianco NL, Jenq KY, Marin J, Dean AJ. Inter-rater reliability of quantifying pleural B-lines using multiple counting methods. J Ultrasound Med. 2013;32(1):115-20.
7. Koenig SJ, Narasimhan M, Mayo PH. Thoracic ultrasonography for the pulmonary specialist. Chest. 2011;140(5):1332-41.
8. Brusasco C, Santori G, Bruzzo E, Tro R, Robba C, Tavazzi G, et al. Quantitative lung ultrasonography: a putative new algorithm for automatic detection and quantification of B-lines. Crit Care. 2019;23(1):288.
9. Alzahrani SA, Al-Salamah MA, Al-Madani WH, Elbarbary MA. Systematic review and meta-analysis for the use of ultrasound versus radiology in diagnosing of pneumonia. Crit Ultrasound J. 2017;9(1):6.

10. Picano E, Gargani L. Ultrasound lung comets: the shape of lung water. Eur J Heart Fail. 2012;14(11):1194-6.
11. Hwang TS, Yoon YM, Jung DI, Yeon SC, Lee HC. Usefulness of transthoracic lung ultrasound for the diagnosis of mild pneumothorax. J Vet Sci. 2018;19(5):660-6.
12. Stigt JA, Groen HJM. Percutaneous ultrasonography as imaging modality and sampling guide for pulmonologists. Respiration. 2014;87(6):441-51.
13. Mathis G. Thoraxsonography—Part 1: Chest wall and pleura. Praxis (Bern 1994). 2004;93(15):615-21.
14. Gorg C, Bert T, Gorg K, Heinzel-Gutenbrunner M. Colour doppler ultrasound mapping of chest wall lesions. Br J Radiol. 2005;78(928):303-7.
15. Mathis G. Thoraxsonography—Part I: Chest wall and pleura. Ultrasound Med Biol. 1997;23(8):1131-9.
16. Manterola HL, Vercio LL, Diaz A, Del Fresno M, Larrabide I. Validation of an open-source tool for measuring carotid lumen diameter and intima-media thickness. Ultrasound Med Biol. 2018;44(8):1873-81.
17. Biswas M, Kuppili V, Saba L, Edla DR, Suri HS, Sharma A, et al. Deep learning fully convolution network for lumen characterization in diabetic patients using carotid ultrasound: a tool for stroke risk. Med Biol Eng Comput. 2019;57(2):543-64.
18. Cinthio M, Jansson T, Eriksson A, Ahlgren AR, Persson HW, Lindstrom K. Evaluation of an algorithm for arterial lumen diameter measurements by means of ultrasound. Med Biol Eng Comput. 2010;48(11):1133-40.
19. Newey VR, Nassiri DK. Online artery diameter measurement in ultrasound images using artificial neural networks. Ultrasound Med Biol. 2002;28(2):209-16.
20. Gutierrez MA, Pilon PE, Lage SG, Kopel L, Carvalho RT, Furuie SS, eds. Automatic measurement of carotid diameter and wall thickness in ultrasound images. In: Computers in Cardiology. Memphis, TN: IEEE; 2002:359-62.
21. Chen J, Li J, Ding X, Wei G, Wang X, Li Q. Automated ultrasound measurement of the inferior vena cava: an animal study. Ultrason Imaging. 2020;42(3):148-58.
22. Chen J, Li J, Ding X, Chang C, Wang X, Ta D. Automated identification and localization of the inferior vena cava using ultrasound: an animal study. Ultrason Imaging. 2018;40(4):232-44.
23. Huang Q, Huang Y, Luo Y, Yuan F, Li X. Segmentation of breast ultrasound image with semantic classification of superpixels. Med Image Anal. 2020;61:101657.
24. Moshavegh R, Hansen KL, Møller-Sørensen H, Nielsen MB, Jensen JA. Automatic detection of B-lines in $In Vivo$ lung ultrasound. IEEE Trans Ultrason Ferroelectr Freq Control. 2019;66(2):309-17.
25. Moshavegh R, Hansen KL, Sorensen HM, Hemmsen MC, Ewertsen MDC, Nielsen MB, et al. Novel automatic detection of pleura and B-lines (comet-tail artifacts) on in vivo lung ultrasound scans. In: Proceedings of SPIE, 2016, vol 9790:1-7.
26. Anantrasirichai N, Hayes W, Allinovi M, Bull D, Achim A. Line detection as an inverse problem: application to lung ultrasound imaging. IEEE Trans Med Imaging. 2017;36(10):2045-56.
27. Lichtenstein DA, Meziere GA. Relevance of lung ultrasound in the diagnosis of acute respiratory failure: the BLUE protocol. Chest. 2008;134(1):117-25.
28. Portney LG, Watkins MP. Foundations of clinical research: applications to practice. 3rd ed. Upper Saddle River: Pearson & Prentice Hall, 2009.
29. Hassanein AS, Mohammad S, Sameer M, Ragab ME. A survey on hough transform, theory, techniques and applications. Comput Sci. 2015;12(1):1-18.
30. Mukhopadhyay P, Chaudhuri BB. A survey of hough transform. Pattern Recognit. 2015;48(3):993-1010.
31. Shapiro LG, Stockman GC. Computer Vision. 1st ed. Prentice Hall: Pearson; 2002.
32. Dietrich C, Hirche T, Schreiber D, Wagner T. Ultrasonography of pleura and lung. Ultraschall Med. 2003;24(05):303-11.
33. Duclos G, Bobbia X, Markarian T, Muller L, Cheyssac C, Castillon S, et al. Speckle tracking quantification of lung sliding for the diagnosis of pneumothorax: a multicentric observational study. Intensive Care Med. 2019;45(9):1212-8.
34. Deans SR. Hough transform from the radon transform. IEEE Trans Pattern Anal Mach Intell. 1981;3(2):185-8.
35. Francisco MJN, Rahal AJ, Vieira FA, Silva PS, Funari MB. Advances in lung ultrasound. Einstein (Sao Paulo). 2016;14(3):443-8.